V European Conference on Computational Fluid Dynamics
ECCOMAS CFD 2010
J. C. F. Pereira and A. Sequeira (Eds)
Lisbon, Portugal,14-17 June 2010

IMPACT OF NASAL GEOMETRY INCLUSION ON NUMERICAL SIMULATION OF FLOW IN HUMAN UPPER AIRWAY

Prihambodo H. Saksono*, Raoul van Loon†, Igor Sazonov† and Perumal Nithiarasu†

*Civil and Computational Engineering Center
School of Engineering, Swansea University,
Singleton Park, Swansea SA2 8PP, United Kingdom
e-mail: p.h.saksono@swansea.ac.uk
†School of Engineering, Swansea University,
Singleton Park, Swansea SA2 8PP, United Kingdom
e-mail: {r.vanloon,i.sazonov,p.nithiarasu}@swansea.ac.uk

Key words: Fluid Dynamics, upper airway, patient-specific modelling, biomedical flows

Abstract. *The use of computational fluid dynamics (CFD) to analyze air flow in respiratory tracts, both healthy and diseased, has increased dramatically in recent years. Most of the analysis are directed towards drug delivery or pollutant transport in the human airway system and some focus on the pathophysiology of the respiratory problems such as asthma, obstructive sleep apnea, etc.*

Initially CFD analysis of the airway flow was carried out on idealised airway geometries. The advances in the medical imaging techniques have increased the use of realistic geometry reconstructed from CT or MRI scan images. However, most of the published works on the numerical simulation of airway flow employ a geometry where the nasal region is excluded. While the use of this geometry gives satisfactory results for drug delivery applications, this is not the case for other applications.

In this work, we use CFD to investigate the implications of the inclusion of the nasal cavity on both global flow pattern and local flow features in a patient-specific upper airway geometry. The geometry is reconstructed from a series of standard CT scans for a healthy subject. The flow is considered to be incompressible and the air is modeled as a Newtonian fluid. The steady Reynolds Averaged Navier-Stokes (RANS) solutions are obtained using the Artificial-Compressibility (AC) Characteristic-Based-Split (CBS) scheme and the one-equation Spalart-Allmaras model is used to describe the transport of the turbulence variable.

1 INTRODUCTION

The use of computational methods to analyze air flow in the human conducting airways, both healthy and diseased, has increased dramatically in recent years. Most of the studies are directed towards drug delivery or pollutant transport in human airway systems and some focus on pathophysiology, such as sleep disorder breathing. Airflow in a human respiratory tract is very complex. The nature of such flows ranges from laminar to transitional to turbulent flow. The main factors that tremendously influence the airflow in human respiratory tracts are the geometry and boundary conditions. Many of the existing CFD analysis of respiratory flow has been carried out on simplified airway geometries. Recently, however, advances in medical imaging techniques and digital image processing have made the use of realistic geometry reconstructed from scans feasible for both extra and intra-thoracic airways.

In the field of particle deposition, the importance of incorporating the oral cavity into the computational domain has been realized early. Most of the recently reported studies on this subject have the oral cavity incorporated into the simplified model of human upper airway. Recent publications by Ma and Lutchen [1], Lin *et.al.* [2] and Jayaraju *et.al.* [3] also incorporate the oral cavity into the realistic geometry that they used. Whilst incorporating the oral cavity gives satisfactory results for drug delivery applications, other applications such as normal breathing and sleep disorder studies, require the inclusion of the more complicated nasal cavity structure.

The inclusion of the nasal cavity into a computational model of flow through a human upper airway has been restricted by the ability of the imaging technique to capture the narrow passages in the nasal cavity in detail and the meshing technique to generate a mesh inside this complex geometry. However, recent growth in the number of published studies on nasal cavity flow [4, 5, 6, 7, 8, 9] show some advances in medical imaging techniques, digital image processing and mesh generation methods. However, high quality CT images are still an issue due to radiation dosage associated with increase in image resolution. Reconstruction and meshing of the airway geometries even now requires a lot of effort and time. Only a very limited number of works on human airway flow include a combination of nasal cavity and trachea. Apart from the work of Lin *et.al.* [2] that underlines the importance of inclusion of the oropharynx and larynx in the analysis of airflow in an airway tree, to the best of authors knowledge there is no published work that highlights how nasal cavity flow affects the flow pattern in the extra-thoracic region of the airway.

Laminar flow conditions in human airway can only be attained under sedentary breathing condition or further down the lung where both airway cross sectional area and air velocity are small enough to facilitate gas exchange in the aveoli. Therefore, we consider the flow to be turbulent in this study. In general, turbulent flow can be simulated using three different approaches, namely, direct numerical simulation (DNS), large eddy simulation (LES), and Reynolds averaged Navier-Stokes (RANS). DNS solves the Navier-Stokes equations directly where all length scales and time scales are resolved. This approach is computationally very expensive and therefore its application is at this moment limited to low-to-moderate Reynolds number flows. In LES, large scale turbulent eddies are resolved directly while the unresolved small-scale eddies are being represented by simplified models. Often both DNS and LES studies need specially arranged structured meshes to obtain a correct solution. This is possible on idealised airway geometries but on patient-specific geometries, such as the one reported in the present work, needs very large computing resources. RANS models on the other hand still have the advantage of being a fast method with reasonable accuracy. Although the RANS models do not resolve turbulent eddies, the dynamics of the turbulent eddies are predicted using semi-empirical models.

Different semi-empirical relations have been proposed to provide a closure for the RANS equations. Among them the one-equation model proposed by Spalart-Allmaras [10] is appealing for solving flow in complex geometries. This is due to the fact that this model is easy to implement, not expensive and naturally lends itself for extending it to more advanced detached eddy simulation (DES). Several studies have been carried out to validate the use of RANS models in respiratory flow with experimental results. However, they provide contradictory conclusions. Stapleton *et.al.* [11] carried out a numerical simulation of particle deposition in an idealised model of the mouth and throat geometry. They state that the characteristics of flow in a complex mouth and throat geometry cause two equation turbulence models to perform poorly. In a recently published article by Mylavarapu *et.al.* [12], the validation was carried out on a patient-specific human upper airway geometry. Comparing the computed and measured wall static pressure they found that the standard $k-\omega$ model provides the best agreement with the experimental measurements and outperforms the LES and the Spalart-Allmaras models. This finding contradicts the popular belief that LES is more accurate and reliable than RANS. Our previous experience on both model and realistic upper human airways clearly shows that the Spalart-Allmaras model performs better at least for steady state flows[13, 14, 15]. Therefore, we use this model to investigate the influence of incorporating nasal cavity.

The main aim of this paper is to analyse the effect of inclusion of the nasal cavity on both the global flow pattern and the local flow features in a patient-specific upper airway. The rest of the paper is organised as follows. Section 2 briefly discusses the process of reconstructing the upper airway geometry of a human subject, mesh generation process followed by a section on RANS equations and the AC-CBS scheme adopted to solve the flow governing equations. In Section 4, we present and discuss the results obtained. Finally, section 5 draws some conclusions.

2 GEOMETRY RECONSTRUCTION AND MESH GENERATION

The first step in creating a patient-specific model is to reconstruct a patient-specific geometry from a series of Magnetic Resonance (MR) or Computed Tomography (CT) images. The geometry used in this study is reconstructed from a series of pre-existing CT images of a patient with healthy airways but who suffered from a different problem. It

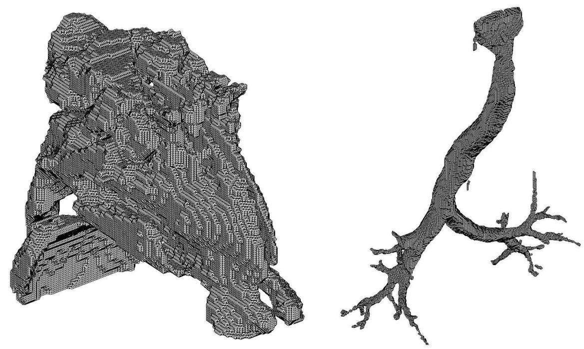

(a) (b)

Figure 1: Airflow through a human upper airway geometry. The initial mesh. (a) nasopharengeal region (b) tracheobronchial region.

comprises 390 slices of 512×512 pixels with 0.877×0.877 mm a spacing of 1.0 mm. The resolution of this scan is considered quite low for CFD puposes, but it is the normal standard for diagnosis in the UK. In order to continuously reconstruct geometries, we prefer to use what is clinically available, rather than using specially arranged high resolution scans.

Despite large differences in density contrast between air and airway tissue, the segmentation process of the upper airway had to be carried out semi-manually using a commercial software (Amira). AMIRA outputs a binary 3D array representing the pixels inside the reconstructed geometry. The surface mesh generation is the most complicated part of the preprocessing. We employed a standard marching cube algorithm to the tracheobronchial region and an advanced version of the marching cube method of Chernyaev [16] was applied to the nasal cavity and nasopharynx. Before applying the advanced version of the marching cube method, the resolution of the nasal part of the geometry was doubled via linear interpolation. This resulted in better gradient approximation and control. Figure 1 shows the initial surface mesh generated using the marching cube methods.

For the numerical simulation, extra parts of the mesh at the exit (bronchi) need to be clipped approximately orthogonal to the centerline of the airways and the clipped planes need to be triangulated. The so-called 'stitching' method [17] is employed to triangulate the outlet planes. In the nasal cavity part, the nasal inlets were triangulated via a marching cube method to form horizontal planes. The triangular elements at both inlet and outlet planes should be marked with appropriate boundary codes to impose appropriate flow boundary conditions. Thus, the resulting surface mesh contains wall triangles and inlet/outlet triangles. The initial mesh is too fine and contains a significant number of very short edges in the nasal part while too coarse in the thoracic part. Therefore, the size of elements in the thoracic part of the initial mesh is made two times smaller dividing every triangle into four similar triangles. Then coarsening and smoothing procedures are applied to the whole mesh using a technique described in [18]. In this technique, the

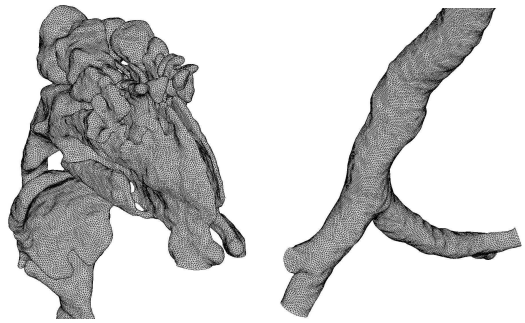

(a) (b)

Figure 2: Surface mesh after the coarsening and smoothing (a) nasal cavity part (b) thoracic part.

shortest edge is determined and contracted into a point. If the surface curvature is locally zero (inlet/outlet planes), the new point to which the edge is contracted is simply its midpoint. If the surface has a finite curvature (wall surface), the point must be put onto the wall surface to prevent the surface mesh from shrinking. Here the airway surface is not described using any analytical surface, such as NURBS, but is defined approximately by the initial location of the mesh nodes. Thus, instead of the G^1 interpolation proposed in [18], an approximate method to determine the new point location is applied, which is easier but gives satisfactory accuracy.

The volume tetrahedron mesh is generated using the Delaunay triangulation method described in [19, 20] prior to application of different mesh improvement techniques. Detailed explanation of techniques that were used to obtained high quality mesh from a segmented geometry can be found in [21]. Figure 2 shows the final geometries used for numerical computation. The final computational mesh for the human upper airway geometry with and without nasal cavity composed of about 2.1 millions tetrahedra and about 1.8 millions tetrahedra, respectively.

3 NUMERICAL SCHEME AND BOUNDARY CONDITIONS

3.1 RANS Equations and AC-CBS Scheme

Even under heavy breathing conditions the flow mach number in human conducting airway is well inside the lower end of the subsonic regime. Therefore, it is widely accepted that airflow through a human respiratory system is assumed to be incompressible. Hence, the Reynolds averaged Navier-Stokes equations, in conservation form, can be written as

Mean continuity

$$\frac{\partial}{\partial x_i}(\rho \bar{u}_i) = 0 \tag{1}$$

Mean momentum

$$\frac{\partial \bar{u}_i}{\partial t} + \frac{\partial}{\partial x_j}(\bar{u}_i \bar{u}_j) = -\frac{1}{\rho}\frac{\partial p}{\partial x_i} + \frac{\partial \tau_{ij}}{\partial x_j} + \frac{\partial \tau_{ij}^R}{\partial x_j} \tag{2}$$

where $\bar{u}_i$ are the mean velocity components, p is the mean pressure and ρ is the density. The mean laminar shear stress tensor is given as

$$\tau_{ij} = \nu \left(\frac{\partial \bar{u}_i}{\partial x_j} + \frac{\partial \bar{u}_j}{\partial x_i} - \frac{2}{3}\frac{\partial \bar{u}_k}{\partial x_k}\delta_{ij} \right)$$

and the Reynolds stress tensor τ_{ij}^R, introduced by Boussinesq's assumption, has the expression

$$\tau_{ij}^R = -\overline{u_i' u_j'} = \nu_T \left(\frac{\partial \bar{u}_i}{\partial x_j} + \frac{\partial \bar{u}_j}{\partial x_i} - \frac{2}{3}\frac{\partial \bar{u}_k}{\partial x_k}\delta_{ij} \right)$$

where ν is the kinematic viscosity of the fluid, ν_T is the turbulent eddy viscosity and δ_{ij} is the Kronecker delta. Using Spalart-Allmaras model, the eddy viscosity is a function of turbulent viscosity $\hat{\nu}$ given by $\nu_T = f_{v1}\hat{\nu}$ in which

$$f_{v1} = \frac{X^3}{X^3 + c_{v1}^3} \quad \text{and} \quad X = \frac{\hat{\nu}}{\nu}.$$

The transport of turbulent viscosity $\hat{\nu}$ is governed by

$$\frac{\partial \hat{\nu}}{\partial t} + \frac{\partial}{\partial x_j}(\bar{u_j}\hat{\nu}) = c_{b1}\hat{S}\hat{\nu} + \frac{1}{\sigma}\left[\frac{\partial}{\partial x_i}(\nu + \hat{\nu})\frac{\partial \hat{\nu}}{\partial x_i} + c_{b2}\left(\frac{\partial \hat{\nu}}{\partial x_i}\right)^2 \right] - c_{w1} f_{w1} \left(\frac{\hat{\nu}}{y}\right)^2 \tag{3}$$

Here, $\hat{S}$ and f_{v2} is defined, respectively, as

$$\hat{S} = S + \left(\frac{\hat{\nu}}{k^2 y^2}\right) f_{v2} \quad \text{and} \quad f_{v2} = 1 - \frac{X}{1 + X f_{v1}}$$

where S is the magnitude of vorticity. The parameter f_w and the constant c_{w1} are, respectively, given by

$$f_w = g\left[\frac{1 + c_{w3}^6}{g^6 + c_{w3}^3}\right]^{\frac{1}{6}} \quad \text{and} \quad c_{w1} = \frac{c_{b1}}{k^2} + \frac{(1 + c_{b2})}{\sigma},$$

where $g = r + c_{w2}(r^6 - r)$ and

$$r = \frac{\hat{\nu}}{\hat{S}k^2 y^2}.$$

The constants are $c_{b1} = 0.1355$, $\sigma = 2/3$, $c_{b2} = 0.622$, $k = 0.41$, $c_{w2} = 0.3$, $c_{w3} = 2$ and $c_{v1} = 7.1$.

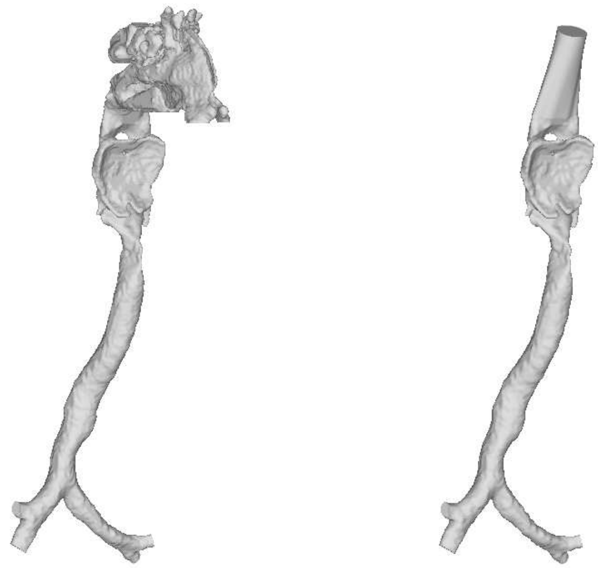

(a) (b)

Figure 3: Human upper airway geometries used for the numerical simulations: (a) Geometry-I (b) Geometry-II

Results presented in this paper were obtained using a class of finite element method (FEM) known as Characteristic-Based Split (CBS) FEM [13, 14, 22, 23, 24, 25, 15]. The CBS scheme is very similar to the original Chorin split [26] and also has similarities with the projection scheme widely employed in incompressible flow calculations. In order to solve the incompressible Navier-Stokes equation efficiently the Artificial Compressibility (AC) method is used in conjunction with the CBS FEM.

In AC-CBS scheme the continuity equation, Equation (1), is replaced by the following equation

$$\frac{1}{\beta^2}\frac{\partial p}{\partial t} + \frac{\partial}{\partial x_i}(\rho \bar{u}_i) = 0 \tag{4}$$

where β is an artificial compressibility parameter.

The scheme then solves Equations (4) and (2) in three steps. In the first step, an intermediate velocity field is obtained, followed by the second step where pressure field is computed and, finally, the velocity field is corrected in the third step. The one equation SA turbulence model is added as a fourth step. The steps of the AC-CBS scheme in its semi-discrete form can be summarised as

Step 1: intermediate momentum

$$\Delta\tilde{U}_i = \tilde{U}_i - U_i^n = \Delta t \left[-\frac{\partial}{\partial x_j}(u_j U_i) + \frac{\partial \tau_{ij}}{\partial x_j} + \frac{\partial \tau_{ij}^R}{\partial x_j} + \frac{\Delta t}{2} u_k \frac{\partial}{\partial x_k}\left(\frac{\partial}{\partial x_j}(u_j U_i) + \right) \right]^n \tag{5}$$

Step 2: pressure

$$\left(\frac{1}{\beta^2}\right)^n p^{n+1} = \left(\frac{1}{\beta^2}\right)^n p^n - \Delta t \left[\frac{\partial U_i^n}{\partial x_i} + \theta_1 \frac{\Delta \tilde{U}_i}{\partial x_i} - \Delta t \theta_1 \frac{\partial}{\partial x_i}\frac{\partial p^n}{\partial x_i} \right] \tag{6}$$

Step 3: momentum correction

$$\Delta U_i = U_i^{n+1} - U_i^n = \Delta \tilde{U}_i - \Delta t \frac{\partial p^n}{\partial x_i} \tag{7}$$

Step 4: transport of turbulence variable

$$\begin{aligned}\hat{\nu}^{n+1} = \hat{\nu}^n + \\ \Delta t \left[-\frac{\partial}{\partial x_i}(\hat{\nu}\bar{u}_i) + c_{b1}\hat{S}\hat{\nu} + \frac{1}{\sigma}\left(\frac{\partial}{\partial x_i}(\nu + \hat{\nu})\frac{\partial \hat{\nu}}{\partial x_i} + c_{b2}\frac{\partial \hat{\nu}}{\partial x_i}\frac{\partial \hat{\nu}}{\partial x_i} \right) - c_{w1} f_{w1} \left(\frac{\hat{\nu}}{y}\right)^2 \right] + \\ \frac{\Delta t^2}{2}\bar{u}_j \left[\frac{\partial}{\partial x_j}\left(\frac{\partial}{\partial x_i}(\bar{u}_i \hat{\nu}) \right) \right]\end{aligned} \tag{8}$$

3.2 Boundary Conditions

In reality, respiratory flow is driven by the pressure difference generated by the deformation of lung tissue. Due to the unavailability of the patient-specific information on outlet pressure evolution during a breathing cycle, standard boundary conditions are prescribed that have been widely used in published works, i.e. a velocity profile at the inlet and a constant pressure at the outlet. The inlet velocity profile can be applied directly at the nares (nostrils) or at inlet of an extension tube attached to the nares. Although prescribing pressure difference is a better approximation to the physical process, the correct flow rate can only be achieved by iteratively adjusting the pressure difference.

To create a physiologically realistic inlet boundary condition, Doorly and co-workers [7, 8, 9] included, the external face of the subject in their patient-specific computational model. In [9], they used this model as a reference to compare two of the most commonly used inflow boundary conditions, namely, imposing inlet velocity profile directly at the nares and imposing the inlet velocity profile to the nares using extension tubes. They found that the use of a tapered extension pipe resulted in a better approximation.

To simplify the geometry reconstruction and mesh generation process we opt out the use of convergent tube at the nares to impose inlet boundary condition. The parabolic velocity profiles are applied directly on both nares. The parabolic profile is generated by solving Poissons equation on the inlet boundary. If in every inlet/outlet we introduce local co-ordinates such that the x and y axis are in the plane of the inlet and the z co-ordinate

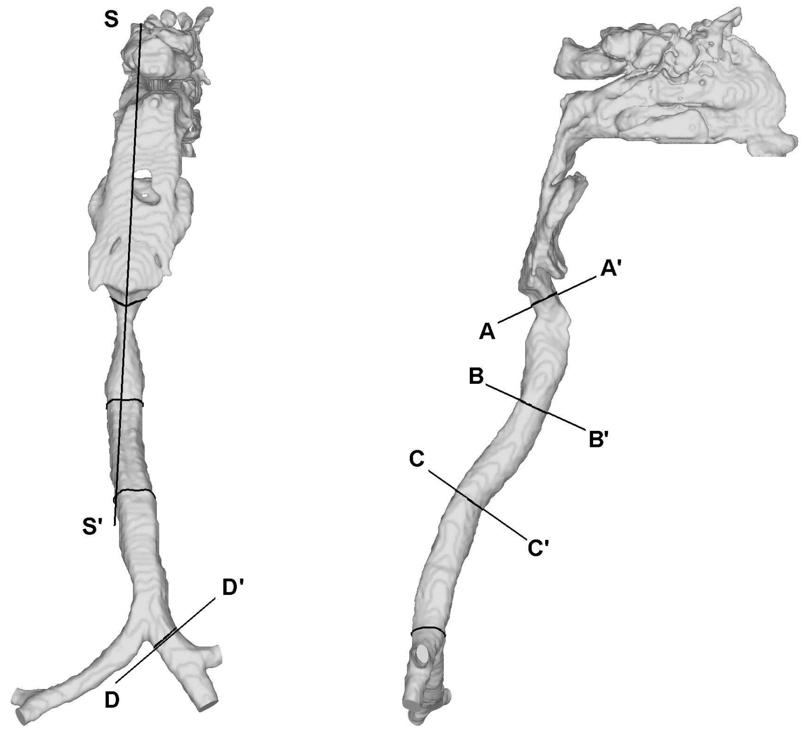

Figure 4: Airflow through a human upper airway geometry. Locations of different cross sections where results will be plotted.

is orthogonal to this plane then the equation for the velocity component normal to the plane reads as

$$\nabla^2 \boldsymbol{u}_n \big|_{\Gamma^{\text{inlet}}} = -\frac{1}{\mu} \partial_z p \big|_{\Gamma^{\text{inlet}}} \tag{9}$$

where $\nabla^2 = \partial_x^2 + \partial_y^2$ is in-plane Laplace operator, $\partial_z p\big|_{\Gamma^{\text{inlet}}}$ is the pressure gradient assumed to be constant across the inlet plane, μ is the dynamic viscosity. The integration is performed by the FE method using the existing triangulation of inlet/outlets. In case of a circular pipe this method gives the parabolic Poiseuille velocity profile, but gives a natural generalization of that profile for more complicated inlet shapes. This way of implementing the inlet/exit boundary conditions clearly reduces the computation required for extension tubes.

4 NUMERICAL SIMULATIONS

To study the impact of a nasal cavity inclusion on the flow pattern in a human upper airway, independent calculations were carried out on geometries with and without the nasal cavity. Geometry I is defined as the model that includes nasal cavity, pharynx, larynx, trachea and the main airway bifurcation with two generations of bronchi.

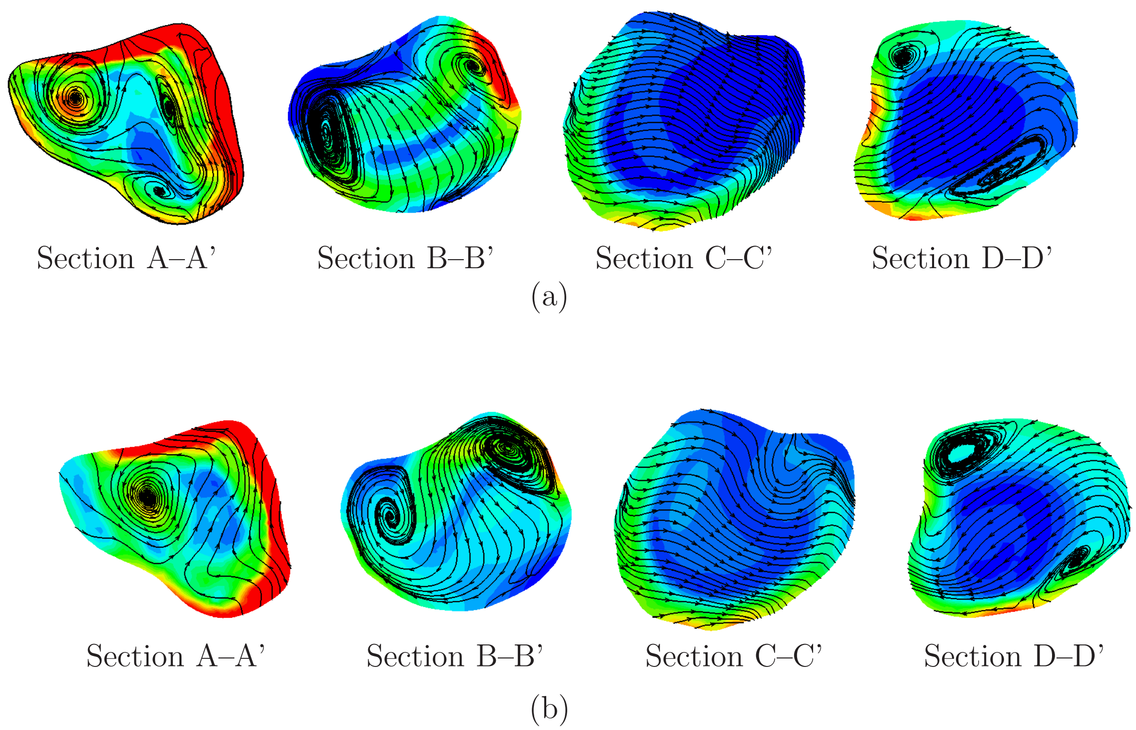

Figure 5: Airflow through a human upper airway geometry.Contours of vorticity magnitude and streamlines at different cross-sections: (a) Geometry I, (b) Geometry II.

Geometry-II is an exact copy of Geometry-I, but excludes the nasal cavity. This latter geometry is created by truncating the geometry just below the nasopharynx. The space occupied by the uvula is one of the geometrical features that needs special attention in Geometry-II. This space divides the air flow in the oropharynx region into two. In Geometry-II the distance between the inlet boundary and this separation region is very close as a consequence directly imposing the velocity profile on the inlet boundary is causing a convergence problem. To minimize the boundary effect on Geometry-II an extension tube is attached at the inlet boundary. Both geometries are shown in Figure 3. Note that the kinematic viscosity of air is considered to be $\nu = 1.69\,\mathrm{cm}^2/\mathrm{s}$ and the flow rate is $Q = 15\,\mathrm{L/min}$.

The first noticeable impact of the inclusion of the nasal cavity is that in Geometry-I, a 90° change in flow direction causes the flow to recirculate and mix much more than in Geometry-II. In addition, inclusion of the nasal cavity makes the flow to develop more secondary flow vortices. This can be clearly seen in Figures 5 and 6. Contours of velocity and streamlines at different cross-sections for both Geometry-I and Geometry-II are depicted in Figure 5. Examination of these plots reveals that the differences in the pattern of secondary flows between the two geometries is significant up to cross section B–B'.

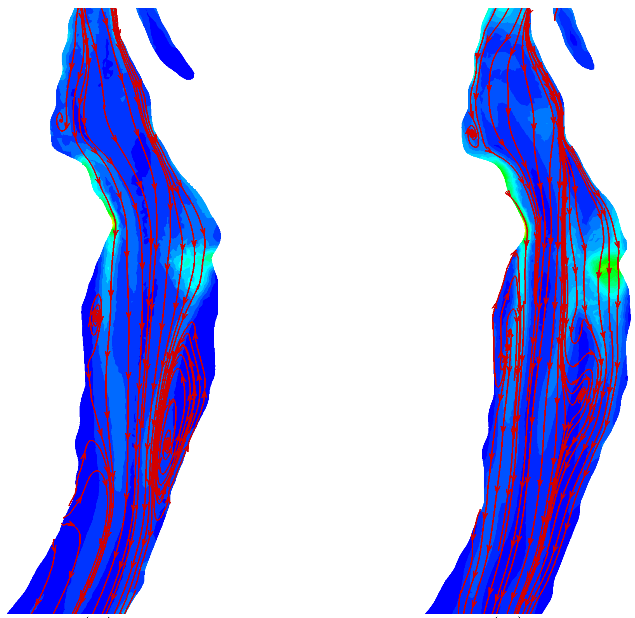

(a) (b)

Figure 6: Airflow through a human upper airway geometry. Contours of vorticity magnitude and streamlines at S-S' section: (a) Geometry-I, (b) Geometry-II.

However, the differences in sagital flow pattern depicted in Figure 6 are substantial. The inclusion of the nasal geometry induces the formation of a stronger recirculation region in the anterior part of the trachea as opposed to the weak posterior one when the nasal geometry is excluded from computation. The differences in the primary flow pattern bring serious implications to modelling the airflow without the nasal cavity [14, 27, 28]. In addition to predicting wrong locations of airway collapse, this can lead to wrong location of particle deposition, when incomplete geometries are used in particle inhalation studies. This also means that the location of negative pressure will be predicted in two completely different locations with and without the nasal cavity.

5 CONCLUSION

In this work, we have presented flow through a complete upper human airway and compared the results with the airway in absence of the nasal cavity. The AC-CBS scheme along with a one-equation turbulence model was used to investigate steady state flow. The following conclusions have been reached from the flow results.

- Incorporating the nasal cavity in the analysis is essential to study the lower part of the upper airway. The results with and without the nasal cavity are dramatically different.
- The selection of flow boundary conditions at the inlet should be carried out carefully. For truly patient-specific studies, spirometry results may be necessary to precisely investigate the flow results.
- The one-equation turbulence model is easy to use, but although the accuracy of this model for recirculating flow was demonstrated in the past, its accuracy for patient-specific geometries has currently not been investigated.

The area of modelling flow through respiratory systems is one of the least researched areas within the biofluid dynamics community. There are several computational and physical issues related to flow modelling in airways. The obvious extension of the present work includes breathing studies, detached eddy simulation and airway collapse studies.

REFERENCES

[1] B. Ma and K. R. Lutchen, An anatomically based hybrid computational model of the human lung and its application to low frequency oscillatory mechanics, *Ann. Biomed. Eng.*, **34**, 1691–1704 (2006)

[2] C. Lin, M. H. Tawhai, G. McLennan, and E. A. Hoffman, Characteristics of the turbulent laryngeal jet and its effect on airflow in the human intra-thoracic airways, Resp. Physiol. Neurobiol., **157**, 295–309 (2007)

[3] S.T. Jayaraju, M. Brouns, S. Verbanck, and C. Lacor, Fluid flow and particle deposition analysis in a realistic extrathoracic airway model using unstructured grids, *J. Aerosol Sci.*, **38**, 494–508 (2007)

[4] C. Croce, R. Fodil, M. Durand, G. Sbirlea-Apiou, G. Caillibotte, J.F. Papon, J.R. Blondeau, A. Coste, D. Isabey and B. Louis, In vitro experiments and numerical simulations of airflow in realistic nasal airway geometry, *Ann. Biomed. Engng.*, **34**, 997–1007 (2006)

[5] G. J. M. Garcia, N. Bailie, D. A. Martins, and J. S. Kimbell, Atrophic rhinitis: a CFD study of air conditioning in the nasal cavity, *J. Appl. Physiol.*, **103**, 1082–1092 (2007)

[6] H. Shi, C. Kleinstreuer, and Z. Zhang, Modeling of inertial particle transport and deposition in human nasal cavities with wall roughness, *J. Aerosol Sci.*, **38**, 398–419 (2007)

[7] D. Doorly, D. J. Taylor, P. Franke, and R. C. Schroter, Experimental investigation of nasal airflow, *Proc. Inst. Mech. Eng. H-J. Eng. Med.*, **222**, 439–453 (2008)

[8] D. J. Doorly, D. J. Taylor, and R. C. Schroter, Mechanics of airflow in the human nasal airways, *Resp. Physiol. Neurobiol.*, **163**, 100–110(2008)

[9] D. J. Taylor, D. J. Doorly, and R. C. Schroter, Inflow boundary profile prescription for numerical simulation of nasal airflow, *J. R. Soc. Interface*, 515-527 (2010)

[10] P.R. Spalart and S.R. Allmaras, A one-equation turbulence model for aerodynamic flows, *AIAA Paper 920439*, (1992)

[11] K. W. Stapleton,E. Guentsch, M. K. Hoskinson, and W. H. Finlay, On the suitability of k-epsilon turbulence modeling for aerosol deposition in the mouth and throat: A comparison with experiment, *J. Aerosol Sci.*, **31**, 739–749 (2000)

[12] G. Mylavarapu, S. Murugappan, M. Mihaescu, M. Kalra, S. Khosla, and E. Gutmark, Validation of computational fluid dynamics methodology used for human upper airway flow simulations, *J. Biomech.*, **42**, 1553–1559 (2009)

[13] P. Nithiarasu, C. B. Liu, and N. Massarotti, Laminar and turbulent flow calculations through a model human upper airway using unstructured meshes, *Commun. Numer. Meth. Engng.*, **23**, 1057–1069 (2007)

[14] P. Nithiarasu, O. Hassan, K. Morgan, N. P. Weatherill, C. Fielder, H. Whittet, P. Ebden, and K. R. Lewis, Steady flow through a realistic human upper airway geometry, *Int. J. Numer. Meth. Fluids*, **57**, 631–651 (2008)

[15] P. Nithiarasu and C-B. Liu, An explicit characteristic based split (cbs) scheme for incompressible turbulent flows, *Comput. Methods Appl. Mech. Engrg.*, **195**, 2961–2982 (2006)

[16] E. V. Chernyaev, Marching cube: Construction of topologically correct isosurfaces, *Technical Report CERN CN 95–17*, CERN (1995)

[17] I. Sazonov, O. Hassan, D. S. Wang, K. Morgan, and N. Weatherill, A stitching method for the generation of unstructured meshes for use with co-volume solution techniques.*Comput. Methods Appl. Mech. Engrg.*, **195**, 1826–1845 (2006)

[18] D. S. Wang, O. Hassan, K. Morgan, and N. P. Weatherill, Enhanced remeshing from stl files with applications to surface grid generation, *Commun. Numer. Meth. Engng.*, **23**, 227–239 (2007)

[19] N. P. Weatherill and O. Hassan, Efficient 3-dimensional Delaunay triangulation with automatic point creation and imposed boundary constrained. *Int. J. Numer. Meth. Engng.*, **37**, 2005–2039, (1994)

[20] O. Hassan, K. Morgan, E.J. Probert and J. Peraire, Unstructured tetrahedral mesh generation for three-dimensional viscous flows, *Int. J. Numer. Meth. Engng.*, **39**, 549–567 (1996)

[21] P. H. Saksono, P. Nithiarasu and I. Sazonov, Computational flow studies in a subject-specific human upper airway using a one-equation turbulence model. Influence of the nasal cavity, *Int. J. Numer. Meth. Engng.* submitted for publication

[22] P. Nithiarasu, An efficient artificial compressibility (ac) scheme based on the characteristic based split (cbs) method for incompressible flows, *Int. J. Numer Meth. Fluids*, **56**, 1815–1845 (2003)

[23] P. Nithiarasu, J.S. Mathur, N.P. Weatherill, and K. Morgan, Three-dimensional incompressible flow calculations using the characteristic based split (cbs) scheme, *Int. J. Numer. Meth. Fluids*, **44**, 1207–29 (2004)

[24] P. Nithiarasu, An arbitrary lagrangian eulerian (ale) method for free surface flow calculations using the characteristic based split (cbs) scheme, *Int. J. Numer. Meth. Fluids*, **48**, 1415–1428 (2005)

[25] P. Nithiarasu, R. Codina, and O.C. Zienkiewicz, The characteristic based split (cbs) scheme − a unified approach to fluid dynamics, *Int. J. Numer. Meth. Engng.*, **66**, 1514–1546 (2006)

[26] A.J. Chorin, Numerical solution of Navier-Stokes equations,*Math. Comput.*, **22**, 745–762 (1968)

[27] M. Mihaescu, S. Murugappan, M. Kalra, S. Khosla, E. Gutmark, Large Eddy Simulation and Reynolds-Averaged NavierStokesmodeling of flow in a realistic pharyngeal airway model: An investigation of obstructive sleep apnea, *J. Biomech.*, **41**, 2279–2288 (2008)

[28] M. Malve, A. Perez, J. L. Lopez-Villalobos, A. Ginel, and M. Doblare, FSI analysis of the coughing mechanism in a human trachea, *Ann. Biomed. Eng.*, **38**, 1556–1565 (2010).